



**HAL**  
open science

# Stability analysis of an equation with two delays and application to the production of platelets

Loïs Boullu, Laurent Pujo-Menjouet, Jacques Bélair

► **To cite this version:**

Loïs Boullu, Laurent Pujo-Menjouet, Jacques Bélair. Stability analysis of an equation with two delays and application to the production of platelets. *Discrete and Continuous Dynamical Systems - Series S*, 2020, 13 (11), pp.3005-3027. 10.3934/dcdss.2020131 . hal-02109546

**HAL Id: hal-02109546**

**<https://inria.hal.science/hal-02109546>**

Submitted on 25 Apr 2019

**HAL** is a multi-disciplinary open access archive for the deposit and dissemination of scientific research documents, whether they are published or not. The documents may come from teaching and research institutions in France or abroad, or from public or private research centers.

L'archive ouverte pluridisciplinaire **HAL**, est destinée au dépôt et à la diffusion de documents scientifiques de niveau recherche, publiés ou non, émanant des établissements d'enseignement et de recherche français ou étrangers, des laboratoires publics ou privés.

# STABILITY ANALYSIS OF AN EQUATION WITH TWO DELAYS AND APPLICATION TO THE PRODUCTION OF PLATELETS

LOÏS BOULLU\*

Univ Lyon, Université Claude Bernard Lyon 1,  
CNRS UMR 5208, Institut Camille Jordan, 43 blvd. du 11 novembre 1918  
F-69622 Villeurbanne cedex, France

LAURENT PUJO-MENJOUET

Univ Lyon, Université Claude Bernard Lyon 1,  
CNRS UMR 5208, Institut Camille Jordan, 43 blvd. du 11 novembre 1918  
F-69622 Villeurbanne cedex, France

JACQUES BÉLAIR

Département de Mathématiques et de statistiques de l'Université de Montréal,  
Pavillon André-Aisenstadt, CP 6128 Succ. centre-ville  
Montréal (Québec) H3C 3J7 Canada

**\* This a preprint version of the article accepted in *Dis. Cont. Dyn. Sys. Ser. S* in 2019.**

ABSTRACT. We analyze the stability of a differential equation with two delays originating from a model for a population divided into two subpopulations, immature and mature, and we apply this analysis to a model for platelet production. The dynamics of mature individuals is described by the following nonlinear differential equation with two delays:  $x'(t) = -\gamma x(t) + g(x(t - \tau_1)) - g(x(t - \tau_1 - \tau_2))e^{-\gamma\tau_2}$ . The method of D-decomposition is used to compute the stability regions for a given equilibrium. The centre manifold theory is used to investigate the steady-state bifurcation and the Hopf bifurcation. Similarly, analysis of the centre manifold associated with a double bifurcation is used to identify a set of parameters such that the solution is a torus in the pseudo-phase space. Finally, the results of the local stability analysis are used to study the impact of an increase of the death rate  $\gamma$  or of a decrease of the survival time  $\tau_2$  of platelets on the onset of oscillations. We show that the stability is lost through a small decrease of survival time (from 8.4 to 7 days), or through an important increase of the death rate (from 0.05 to 0.625 days<sup>-1</sup>).

---

2010 *Mathematics Subject Classification.* Primary: 34K13, 34K18 ; Secondary: 92D25.

*Key words and phrases.* Platelets, oscillations, stability, two delays, D-decomposition, centre manifold analysis.

LB was supported by the LABEX MILYON (ANR-10-LABX-0070) of Université de Lyon, within the program “Investissements d’Avenir” (ANR-11-IDEX-0007) operated by the French National Research Agency (ANR). Also, LB is supported by a grant of Région Rhône-Alpes and benefited of the help of the France Canada Research Fund, of the NSERC and of a support from MITACS. JB acknowledges support from NSERC [Discovery Grant].

\* Corresponding author: lboullu@gmail.com.

**1. Introduction.** Differential equations with two delays arise when a system includes two “non-instantaneous” processes requiring a finite time to be completed. Take for example a population composed of immature individuals and mature individuals, such that immature individuals become mature after a time  $\tau_1$  and mature individuals die after having been mature for a time  $\tau_2$ . If we assume that at any time  $t \geq 0$ , the rate of production of immature individuals is a positive function  $g$  of the total population  $x(t)$  of mature individuals, then the dynamics of  $x$  is described by the following differential equation:

$$x'(t) = g(x(t - \tau_1)) - g(x(t - \tau_1 - \tau_2)).$$

Adding a random destruction rate  $\gamma$ , Bélair *et al.* [2] formulated a model for the production of platelets whose dynamics are given by

$$x'(t) = -\gamma x(t) + g(x(t - \tau_1)) - g(x(t - \tau_1 - \tau_2))e^{-\gamma\tau_2}. \quad (1.1)$$

The derivation of this equation from the structured PDEs describing the two populations can be found in [10]. The immature cells are megakaryocytes, whose production rate is a decreasing function of the platelet count, and which release between 1000 and 3000 platelets after a maturation time  $\tau_1$ . In the context of a disease called “cyclic thrombocytopenia” [11], Bélair *et al.* [2] found that in the case where the function  $g$  has a bell-shape given by  $g(x) := f_0 \frac{\theta^n x}{\theta^n + x^n}$ , increasing the death rate  $\gamma$  induces a de-stabilization of the positive equilibrium. Equation (1.1) with the same function  $g$  has also been studied by El-Morshedy *et al.* [10] as authors identified conditions for the global stability of either the trivial equilibrium or the positive equilibrium.

Notice that if  $x^*$  is an equilibrium of (1.1), then the corresponding characteristic equation is given by

$$\lambda + \gamma - g'(x^*)e^{-\lambda\tau_1} + g'(x^*)e^{-\gamma\tau_2}e^{-\lambda(\tau_2+\tau_1)} = 0, \quad (1.2)$$

a particular case of the general form

$$\lambda + A + Be^{-\lambda r_1} + Ce^{-\lambda r_2} = 0. \quad (1.3)$$

Stability with respect to  $A$ ,  $B$  and  $C$  has been studied by Mahaffy *et al.* [21] in the case where  $r_1 > r_2$ , and by Mahaffy & Busken [7] when  $r_1 = nr_2$  with  $n \in \mathbb{N}$ . Besse also studied this general form [4], although with respect to  $A$  and  $B$  and in the case where  $A, B \geq 0$  and  $-\pi/r_1 \leq C \leq 0$ . Bélair & Campbell [1] studied the case where  $A = 0$  and  $B = 1$ : they identified the stability regions in the  $(A, r_2)$  plan, and were able to show that increasing  $r_1$  leads to the separation of the stability region into multiple disconnected regions. Although Equation (1.2) constitutes a more complex case than the one treated by Mahaffy & Busken [7], as  $C$  depends on  $r_1, r_2$  and  $A$ , this specificity reduces the number of parameters by one, allowing for a more complete analysis of the role each parameter plays in shaping the regions of stability.

The assumption of a regulation of platelet count relying on variable megakaryocyte production was recently studied by Boullu *et al.* [6]. Using a non constant maturation rate for megakaryoblasts (cells from which megakaryocytes originate), this lead to a system of two delay-differential equations. The authors showed that increasing the death rate of megakaryoblasts could induce periodic solutions. But the use of random-only platelet death prevented from studying the effect of an increased destruction of platelets. The objective of this paper is to study in detail the local stability of the equilibria of (1.1). Then, (1.1) is used as a simplification of the

model presented in [6] to study the impact of an increased destruction of platelets on the stability, through the increase of the random death rate  $\gamma$  as well as through the decrease of survival time  $\tau_2$ . Indeed, both the increase of  $\gamma$  and the decrease of  $\tau_2$  may be induced by the presence of platelet-specific antibodies [12, 19, 22].

In Section 2, we perform the linear stability analysis of (1.1). Since for  $B := g'(x^*)\tau_1 = 0$  the non-trivial equilibrium is locally asymptotically stable, we study the existence of purely imaginary eigenvalues as  $|B|$  increases from zero for different values of  $\tau := \tau_2/\tau_1$  and  $A := \gamma\tau_1$ . Following the D-decomposition approach [13], we obtain implicit expressions for  $\tau$ ,  $A$  and  $B$  allowing us to numerically plot the curves where  $\lambda = i\omega$  is a root of (1.2), in both the  $(\tau, B)$  and  $(A, B)$  planes. In order to determine whether the existence of a pair of purely imaginary eigenvalues implies a change in the number of eigenvalues with positive real parts, we study the sign of the derivative of  $\text{Re}(\lambda)$  with respect to one of the parameters. This enables us to associate each region to a number of eigenvalues with positive real part. In order to determine the nature of the changes of dynamic associated with a loss of stability, we perform a centre manifold analysis for the steady-state bifurcation and for a single Hopf bifurcation in Section 3. Then, we notice that the crossing of stability curves indicates that complex behaviours, such as tori, are possible. To identify parameters associated with these complex behaviours we perform the centre manifold analysis of a double Hopf bifurcation in Section 4. Finally, the results of Section 2 are applied in Section 5 to (1.1) the equation for platelet count presented above.

## 2. Linear stability analysis.

**2.1. Curves associated with purely imaginary eigenvalues.** In order to decrease the complexity further, we rescale time in units of one of the delays, setting  $s = t/\tau_1$ . Thus, if  $z$  is a solution of the linearization of (1.1) about one of its equilibrium  $x^*$ , that is,

$$z'(t) = -\gamma z(t) + g'(x^*)z(t - \tau_1) - g'(x^*)z(t - \tau_1 - \tau_2)e^{-\gamma\tau_2}. \quad (2.1)$$

Then we define a function  $y$  as  $y(s) = z(s\tau_1)$  and obtain

$$\begin{aligned} y'(s) &= -\gamma\tau_1 y(s) + g'(x^*)\tau_1 y(s-1) - g'(x^*)\tau_1 y(s-1-\tau_2/\tau_1)e^{-\gamma\tau_2}, \\ &= -Ay(s) + B[y(s-1) - e^{-\gamma\tau_2}y(s-1-\tau)], \end{aligned} \quad (2.2)$$

where  $A = \gamma\tau_1 > 0$ ,  $B = g'(x^*)\tau_1$  and  $\tau = \tau_2/\tau_1 > 0$ . Notice that  $\gamma\tau_2 = A\tau$ , such that the corresponding characteristic equation is written

$$\lambda = -A + B[e^{-\lambda} - e^{-A\tau}e^{-\lambda(1+\tau)}]. \quad (2.3)$$

For  $B = 0$ , Equation (2.3) becomes  $\lambda = -A < 0$ : there is only one eigenvalue and it is real and negative, therefore the equilibrium is locally asymptotically stable. Because the number of eigenvalues  $\lambda$  of Equation (2.3) with  $\text{Re}(\lambda) > 0$  can change only by a crossing of  $\lambda$  through the imaginary axis, the boundaries of the stability regions in the plane of parameters correspond to the values such that there exists a  $\omega \in \mathbb{R}_+$  with  $\lambda = i\omega$  solution of (2.3). For such a  $\lambda$ , (2.3) becomes

$$0 = -i\omega - A + B(e^{-i\omega} - e^{-A\tau - i\omega(1+\tau)}). \quad (2.4)$$

In the case  $\omega = 0$ , (2.4) leads to

$$0 = -A + B(1 - e^{-A\tau}),$$

so that  $\lambda = 0$  is an eigenvalue if and only if  $B = \frac{A}{1-e^{-A\tau}}$ . If  $\lambda = i\omega \neq 0$ , we need to separate real and imaginary parts:

$$\begin{cases} -A &= B[\cos \omega - e^{-A\tau} \cos(\omega(1+\tau))], \\ \omega &= B[-\sin \omega + e^{-A\tau} \sin(\omega(1+\tau))]. \end{cases} \quad (2.5)$$

For  $B \neq 0$ , we divide one equality by the other to obtain

$$\frac{\omega}{A} = \frac{-\sin \omega + e^{-A\tau} \sin(\omega(1+\tau))}{\cos \omega - e^{-A\tau} \cos(\omega(1+\tau))}, \quad (2.6)$$

and when  $\omega$ ,  $A$  and  $\tau$  are known,  $B$  is given by

$$B = \frac{A}{\cos \omega - e^{-A\tau} \cos(\omega(1+\tau))}. \quad (2.7)$$

In order to determine whether the pair of purely imaginary eigenvalues corresponds to an increase or a decrease in the number of eigenvalues with positive real parts, we compute both  $\frac{d \operatorname{Re} \lambda}{dA}(A)$  and  $\frac{d \operatorname{Re} \lambda}{d\tau}(\tau)$ , then evaluate the transversality condition, that is whether the corresponding derivatives are positive or not.

## 2.2. Transversality conditions.

2.2.1. *With respect to A.* We consider  $\lambda = \alpha + i\omega \in \mathbb{C}$ ,  $A, \tau \in \mathbb{R}_+^*$  and  $B \in \mathbb{R}$ . Differentiating (2.3) with respect to  $A$  gives

$$\frac{d\lambda}{dA} = -1 - Be^{-\lambda} \frac{d\lambda}{dA} + B\left[\tau + (1+\tau) \frac{d\lambda}{dA}\right] e^{-A\tau} e^{-\lambda(1+\tau)},$$

and  $\frac{d}{dA} e^{-A\tau - \lambda(A)(1+\tau)} = (-\tau - \lambda'(A)(1+\tau)) e^{-A\tau - \lambda(A)(1+\tau)}$ , which implies

$$(1 + Be^{-\lambda} - B(1+\tau)e^{-A\tau} e^{-\lambda(1+\tau)}) \frac{d\lambda}{dA} = -1 + B\tau e^{-A\tau} e^{-\lambda(1+\tau)},$$

and thus

$$\frac{d\lambda}{dA} = \frac{-1 + B\tau e^{-A\tau} e^{-\lambda(1+\tau)}}{1 + Be^{-\lambda} - B(1+\tau)e^{-A\tau} e^{-\lambda(1+\tau)}}.$$

From (2.3) we have  $Be^{-A\tau} e^{-\lambda(1+\tau)} = -\lambda - A + Be^{-\lambda}$  hence the above is written

$$\frac{d\lambda}{dA} = \frac{-1 + \tau(-\lambda - A + Be^{-\lambda})}{1 + Be^{-\lambda} - (1+\tau)(-\lambda - A + Be^{-\lambda})} = \frac{-1 - \tau(\lambda + A - Be^{-\lambda})}{1 - \tau Be^{-\lambda} + (1+\tau)(\lambda + A)},$$

such that for  $\lambda = i\omega$  we have

$$\begin{aligned} \frac{d\lambda}{dA} &= \frac{-1 - \tau i\omega - \tau A + \tau B(\cos \omega - i \sin \omega)}{1 - \tau B(\cos \omega - i \sin \omega) + (1+\tau)(i\omega + A)} \\ &= \frac{[-1 - \tau A + \tau B \cos \omega] - i\tau[\omega + B \sin \omega]}{[1 + (1+\tau)A - \tau B \cos \omega] + i[(1+\tau)\omega + \tau B \sin \omega]}. \end{aligned}$$

Using the general decomposition  $\frac{x+iy}{u+iv} = \frac{xu+yv}{u^2+v^2} + i\frac{yu-xv}{u^2+v^2}$  of any complex number, we obtain the sign of  $\frac{d \operatorname{Re} \lambda}{dA}$  as the sign of

$$\begin{aligned} S_A(\omega, A, B, \tau) &= -1 - (1+2\tau)A - B^2\tau^2 + B\tau(2 + (1+2\tau)A) \cos \omega \\ &\quad - \tau(1+\tau)(A^2 + \omega^2) - \omega\tau(1+2\tau)B \sin \omega. \end{aligned}$$

Figure 2.1 represents in the  $(A, B)$  plane, for  $\tau = 1$ , the graph of the solutions of (2.6), (2.7) as a parametrized curve in  $\omega > 0$ . The branches of this curve delimit the stability regions. The boundaries of the stability region do not qualitatively change with  $\tau$ . From the graph, we note that  $\frac{d \operatorname{Re} \lambda}{dA} < 0$  at all points  $(A(\omega), B(\omega))$ . That

is, stability is lost when the parameters are moved from right to left, *i.e.* when  $A$  decreases, so that exiting the region of stability may give rise to a Hopf bifurcation.

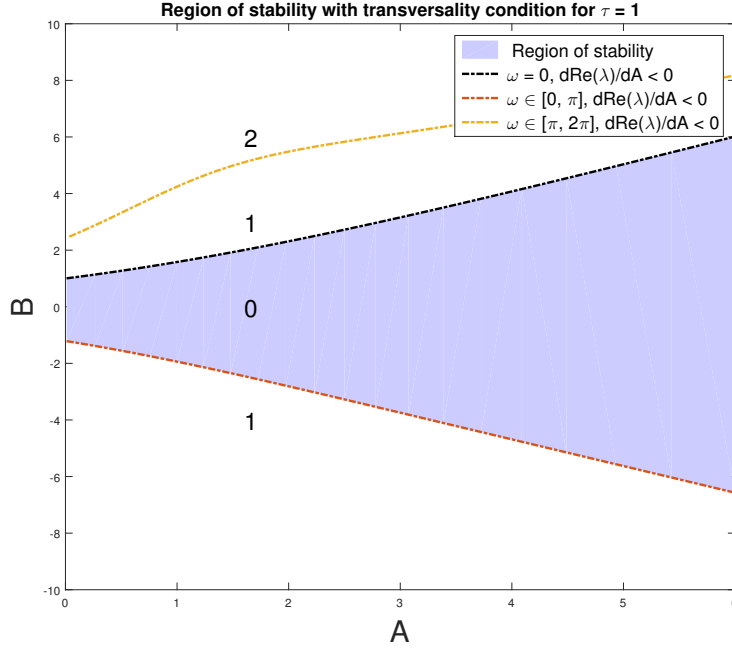


FIGURE 2.1. Region of stability for the null solution of (2.1) with  $\tau = 1$ . The numbers indicate the number of pairs of eigenvalues with positive real parts. The graph is the same for any positive  $\tau$ .

2.2.2. *With respect to  $\tau$ .* We consider again  $\lambda = \alpha + i\omega \in \mathbb{C}$ ,  $A, \tau \in \mathbb{R}_+^*$  and  $B \in \mathbb{R}$ . Differentiating (2.3) with respect to  $\tau$  gives

$$\frac{d\lambda}{d\tau} = -Be^{-\lambda} \frac{d\lambda}{d\tau} + B \left[ A + \lambda + (1 + \tau) \frac{d\lambda}{d\tau} \right] e^{-A\tau} e^{-\lambda(1+\tau)},$$

and as  $\frac{d}{d\tau} e^{-\lambda(\tau)(1+\tau)} = (-\lambda'(\tau)(1 + \tau) - \lambda(\tau)) e^{-\lambda(\tau)(1+\tau)}$ , we obtain

$$\frac{d\lambda}{d\tau} = \frac{B(A + \lambda)e^{-A\tau} e^{-\lambda(1+\tau)}}{1 + Be^{-\lambda} - B(1 + \tau)e^{-A\tau} e^{-\lambda(1+\tau)}}.$$

From (2.3) we have  $Be^{-A\tau} e^{-\lambda(1+\tau)} = -\lambda - A + Be^{-\lambda}$  hence the above is written

$$\frac{d\lambda}{d\tau} = \frac{(A + \lambda)(-\lambda - A + Be^{-\lambda})}{1 - \tau Be^{-\lambda} - (1 + \tau)(-\lambda - A)},$$

which for  $\lambda = i\omega$  becomes

$$\begin{aligned} \frac{d\lambda}{d\tau} &= \frac{(i\omega + A)(-i\omega - A + B(\cos \omega - i \sin \omega))}{1 - B\tau(\cos \omega - i \sin \omega) + (A + i\omega)(1 + \tau)} \\ &= \frac{[A(-A + B \cos \omega) + \omega(\omega + B \sin \omega)] + i[-2A\omega + B(\omega \cos \omega - A \sin \omega)]}{[1 - B\tau \cos \omega + A(1 + \tau)] + i[B\tau \sin \omega + \omega(1 + \tau)]}. \end{aligned}$$

Using the same decomposition as above, we get the sign of  $\frac{d\operatorname{Re}\lambda}{d\tau}$  as the sign of

$$S_\tau(\omega, A, B, \tau) = \omega^2 - A(A + A^2(1 + \tau) + \omega^2(1 + \tau) + B^2\tau) + (A + (2\tau + 1)A^2 + \omega^2)B \cos \omega + (1 - 2A\tau)\omega B \sin \omega.$$

We showed above that on the curve corresponding to  $\omega = 0$ , that  $B = \frac{A}{1 - e^{-A\tau}} > 0$ . A simple calculation implies that the sign of  $\frac{d\operatorname{Re}\lambda}{d\tau}$  is given by  $\frac{1+A}{1+A+A\tau} - e^{-\tau A}$  which is always positive when both  $A$  and  $\tau$  are strictly positive. This corresponds to a steady-state bifurcation.

Figures 2.2–2.5 represent the stability regions for  $A = 0.2$ ,  $A = 0.55$ ,  $A = 1$  and  $A = 2$  respectively. Notice that for  $A = 0.2$  and  $A = 0.55$ , the curves show some loops, and the transversality condition indicates that entering such loops from the left implies the gain of an eigenvalue with positive real part, while exiting the same implies the loss of this eigenvalue.

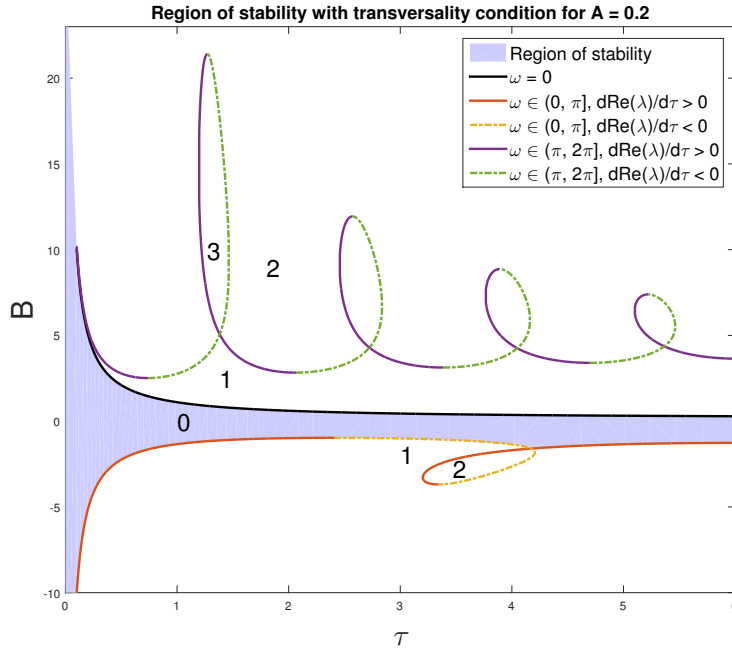


FIGURE 2.2. Region of stability for the null solution of (2.1) with  $A = 0.2$ . The numbers indicate the number of pairs of eigenvalue with positive real parts.

**Remark 1:** in each graphs, we notice that  $\frac{d\operatorname{Re}\lambda}{d\tau} > 0$  at a point  $(\tau, B)$  if and only if the implicit curve  $B \mapsto \omega(B)$  is concave at this point. Verifying this requires to compute the corresponding second derivative, which is out of the scope of this paper and left for a future work. From the graphs again, we assume that there exists a value  $A_0$  such that if  $A \geq A_0$ , then for all points of the plane  $(\tau, B)$  there exists no more than one positive value of  $\omega$  such that  $(\omega, A, \tau, B)$  satisfies (2.5), that is no curve crosses itself or another branch).

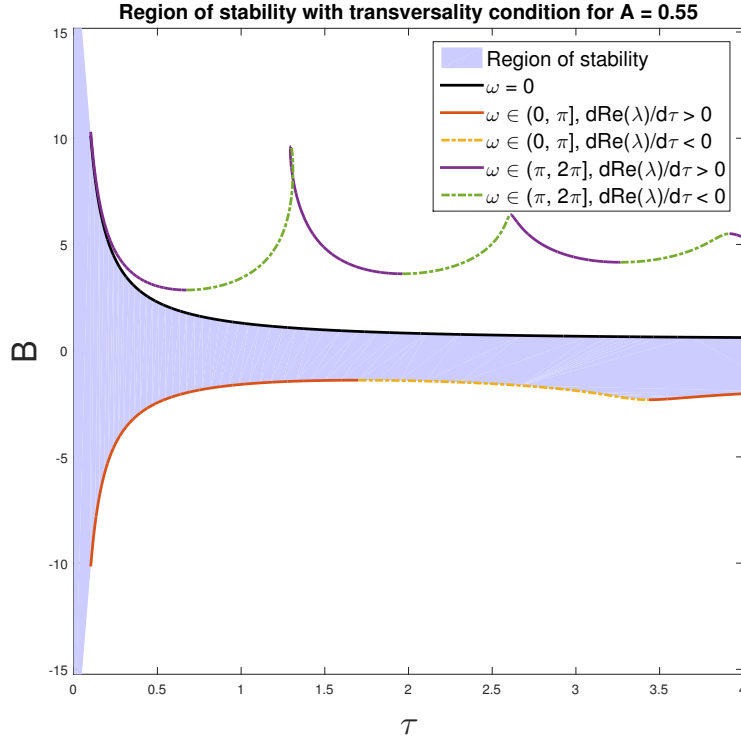


FIGURE 2.3. Region of stability for the null solution of (2.1) with  $A = 0.55$ .

**Remark 2:** to show that the branch for  $\omega = 0$  is always below the other branches corresponding to positive values of  $\omega$ , we study the consequences of  $B < \frac{A}{1-e^{-A\tau}}$ , which implies

$$\begin{cases} -A + B[\cos \omega - e^{-A\tau} \cos(\omega(1 + \tau))] \\ < -\frac{A}{1-e^{-A\tau}}(1 - \cos \omega - (1 - \cos(\omega(1 + \tau)))e^{-A\tau}), \\ -\omega + B[-\sin \omega + e^{-A\tau} \sin(\omega(1 + \tau))] \\ < -\omega(1 + \frac{A}{\omega} \sin \omega - (1 + \frac{A}{\omega} \sin(\omega(1 + \tau)))e^{-A\tau}). \end{cases}$$

Numerically we see that if  $A$  and  $\tau$  are such that  $1 - \cos \omega - (1 - \cos(\omega(1 + \tau)))e^{-A\tau} < 0$  for some  $\omega \in [0, 2\pi]$ , then  $1 + \frac{A}{\omega} \sin \omega - (1 + \frac{A}{\omega} \sin(\omega(1 + \tau)))e^{-A\tau} > 0$ , but an analytical proof is still an open problem. An other open problem is to prove that if  $n \leq m$  and  $(\tau_0, B_0)$  is a point of a curve associated with  $\omega \in [2n\pi, (2n + 1)\pi]$  (resp.  $\omega \in [(2n + 1)\pi, 2(n + 1)\pi]$ ) then if  $(\tau_0, B)$  is a point of a curve associated with  $\omega \in [2m\pi, 2(m + 1)\pi]$  (resp.  $\omega \in [(2m + 1)\pi, 2(m + 1)\pi]$ ) we have  $|B_0| \leq |B|$ .

In the next section we perform a centre manifold analysis for the bifurcation for  $B > 0$  (with  $\lambda = 0$ , a steady-state bifurcation) and for the bifurcation for  $B < 0$  (a Hopf bifurcation).

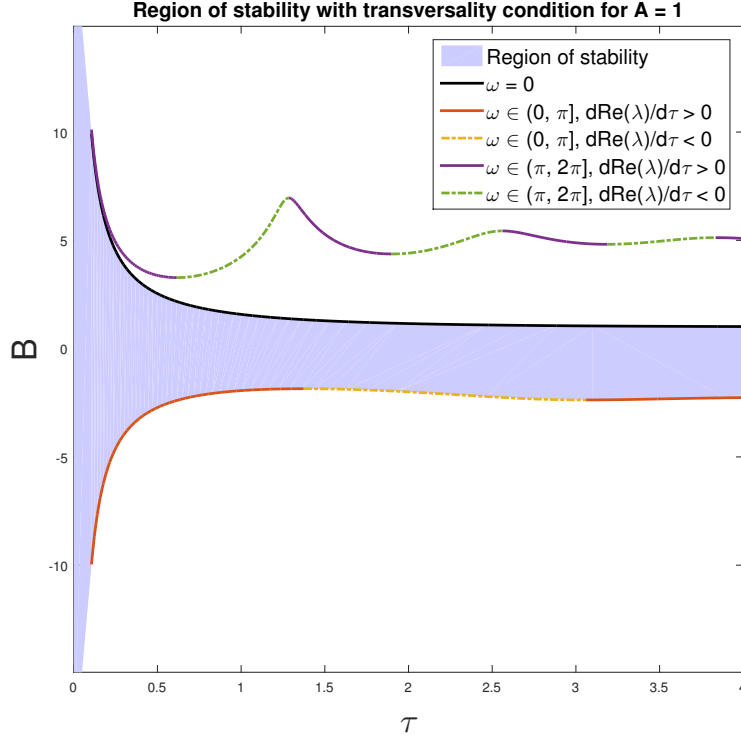


FIGURE 2.4. Region of stability for the null solution of (2.1) with  $A = 1$ .

**3. Centre manifold analysis for simple bifurcations.** When an eigenvalue with positive real part appears through a steady-state bifurcation, the change of stability is generically of one of two types. Either one new locally stable equilibrium point appears, in which case the bifurcation is called “transcritical”, or two new locally stable equilibrium points appear, in which case the bifurcation is called “pitchfork bifurcation”. Similarly, when a pair of eigenvalues with positive real parts appears through a Hopf bifurcation, the change in stability is generically of one of two types. If a stable limit cycle appears when the Hopf bifurcation occurs, it is said to be a “supercritical Hopf bifurcation”, and if an unstable limit cycle disappears when the Hopf bifurcation occurs, it is said to be a “subcritical Hopf bifurcation”. In both instances, to determine the type of the bifurcation we can perform a centre manifold analysis for the steady-state bifurcation and for simple Hopf bifurcation.

**3.1. Theoretical basis for centre manifold analysis (from [8]).** We consider the general delay differential equation with two delays expressed as

$$x'(t) = L(x(t), x(t - \tau_1), x(t - \tau_2)) + f(x(t), x(t - \tau_1), x(t - \tau_2)), \quad (3.1)$$

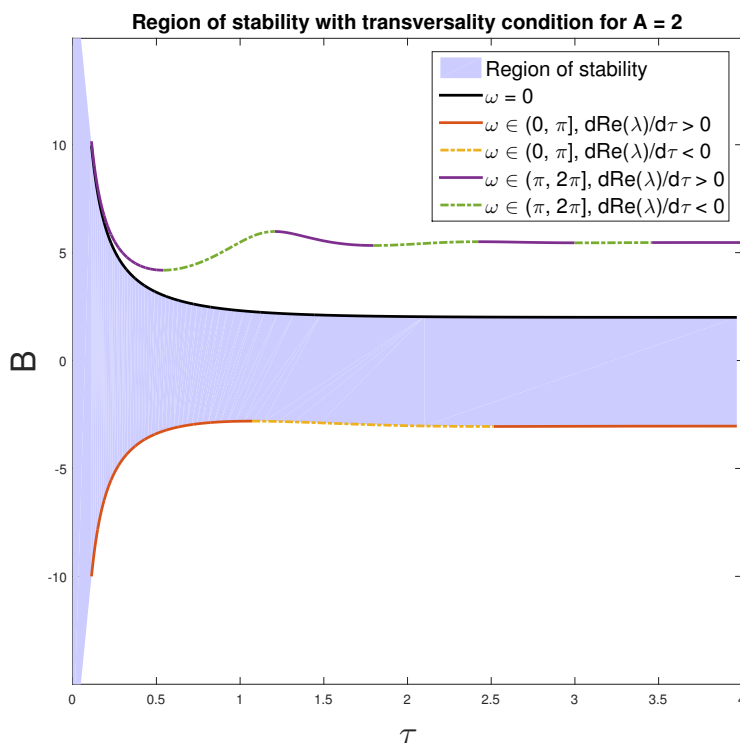


FIGURE 2.5. Region of stability for the null solution of (2.1) with  $A = 2$ .

where  $\tau_1, \tau_2 \geq 0$ ,  $L : \mathbb{R}^3 \rightarrow \mathbb{R}$  a linear operator and  $f : \mathbb{R}^3 \rightarrow \mathbb{R}$ . The linear restriction of the equation is therefore

$$x'(t) = Ax(t) + Bx(t - \tau_1) + Cx(t - \tau_2). \quad (3.2)$$

At a point in parameter space where (3.2) possesses  $m$  eigenvalues with zero real parts, all the other eigenvalues having negative real parts, there exists an  $m$ -dimensional invariant manifold  $C = P \oplus Q$  in the state space. The long term behavior of solutions of the nonlinear equation is well approximated by the flow in this manifold. The flow on this centre manifold is given by  $x(t) = x_t(0)$ , where  $x_t(\theta)$  is a solution of (3.2) satisfying

$$x_t(\theta) = \Phi \mathbf{z}(t) + h(\theta, \mathbf{z}(t)),$$

where  $\Phi$  is a basis for  $P$ ,  $h \in Q$  and  $\mathbf{z}$  satisfies the ordinary differential equation

$$\dot{\mathbf{z}}(t) = \mathcal{B}\mathbf{z}(t) + \mathbf{b}f(\Phi(\theta)\mathbf{z} + \mathbf{h}(\theta, \mathbf{z}(t))). \quad (3.3)$$

Here,  $\mathcal{B}$  is the  $(m \times m)$  matrix of eigenvalues with null real part. To specify  $\mathbf{b}$ , we introduce the bilinear form associated to (3.2):

$$\langle \psi, \phi \rangle = \psi(0)\phi(0) + B \int_{-\tau_1}^0 \psi(\xi + \tau_1)\phi(\xi) d\xi + C \int_{-\tau_2}^0 \psi(\xi + \tau_2)\phi(\xi) d\xi. \quad (3.4)$$

Then,  $\mathbf{b}$  is given by  $\Psi(0)$  where  $\Psi = \langle \Phi^T, \Phi \rangle^{-1} \Phi$  (or  $\langle \Psi, \Phi \rangle = 1$ ).

We now perform the centre manifold analysis for the steady-state bifurcation.

**3.2. Steady-state bifurcation.** In order to study the bifurcation corresponding to the branch  $\lambda = 0$ , we use the result of Song & Jiang on a general delay differential equation ([26], Theorem 1).

We use a rescaled version of (1.1):

$$x'(t) = -Ax(t) + g(x(t-1)) - g(x(t-1-\tau))e^{-A\tau}. \quad (3.5)$$

with  $A, \tau > 0$ , which yields the characteristic equation

$$\lambda = -A + B[e^{-\lambda} - e^{-A\tau}e^{-\lambda(1+\tau)}]. \quad (3.6)$$

with  $B = g'(x^*)$  and  $x^*$  is an equilibrium of (3.5). We introduce the variable  $\mu$  defined as  $\mu := B - \frac{A}{1-e^{-A\tau}}$ , such that for  $\mu = 0$ ,  $\lambda = 0$  is a root of (3.6). Therefore, we choose  $\Phi = \phi(\theta) := 1$  as a basis of  $P$ , and given (3.4),  $\langle \Psi, \Phi \rangle = 1$  implies that

$$\Psi = \psi(\theta) := \frac{1}{1 + B(1 - e^{-A\tau}(1 + \tau))} \Big|_{\mu=0} = \frac{1}{1 + A},$$

is a basis of  $P^*$  the dual space of  $P$ .

The components of the decomposition of (3.5) as  $x'(t) = L(\mu)(x_t) + F(x_t, \mu)$  are given by

$$\begin{aligned} L(\mu)(\phi) &= -A\phi(0) + \left(\mu + \frac{A}{1 - e^{-A\tau}}\right)(\phi(-\tau) - e^{-A\tau}\phi(-1 - \tau)), \\ F(\phi, \mu) &= g(\phi(-1)) - g(\phi(-1 - \tau))e^{-A\tau} \\ &\quad - \left(\mu + \frac{A}{1 - e^{-A\tau}}\right)(\phi(-1) - e^{-A\tau}\phi(-1 - \tau)). \end{aligned}$$

We then compute the linear term  $L_1$  of the Taylor expansion of  $L$  and the second term  $F_2$  of the Taylor expansion of  $F$  on  $\Phi x + y$  where  $x \in \mathbb{R}$  and  $y \in Q$  :

$$\begin{aligned} L_1(\phi) &= \phi(-1) - e^{-A\tau}\phi(-1 - \tau) \\ F_2(\Phi x + y, \mu) &= \left( (x - x^* + y(-1))^2 - (x - x^* + y(-1 - \tau))^2 e^{-\tau A} \right) g''(x^*), \end{aligned}$$

and writing  $F_2(\Phi x + y, \mu) = A_2(x - x^*)^2 + H_2(\Phi x, y) + O(|y|^2)$  gives  $A_2 = (1 - e^{-\tau A})g''(x^*)$ .

We write  $\xi := \phi(\theta) = 1$ ,  $\eta := \psi(\theta) = \frac{1}{1+A} > 0$ ,  $L_1(\xi) = 1 - e^{-A\tau} > 0$ , such that according to Song & Jiang [26], the normal form for the steady-state bifurcation is given by

$$\begin{aligned} \dot{x} &= \eta L_1(\xi)\mu x + \frac{1}{2}\eta A_2 x^2 + O(x^3, \mu|(x, \mu)|^2) \\ &= \frac{1 - e^{-A\tau}}{1 + A}\mu x + \frac{1}{2} \frac{(1 - e^{-A\tau})g''(x^*)}{1 + A} x^2 + O(x^3, \mu|(x, \mu)|^2). \end{aligned} \quad (3.7)$$

Furthermore, using Theorem 1 of [26] we obtain the following result:

**Theorem 3.1.** *If  $0 \geq B = B_0 := \frac{A}{1-e^{-A\tau}}$ , then  $\lambda = 0$  is an eigenvalue of (3.6) and there are no other eigenvalues with zero real part. Also, the constant solution  $x^*$  of (3.5) is locally asymptotically stable for  $B < B_0$  and unstable for  $B > B_0$ .*

*Furthermore, if  $g''(x^*) \neq 0$ , then the constant solution  $x^*$  with  $B = B_0$  is stable and equation (3.5) undergoes a transcritical bifurcation at the critical value  $B = B_0$ .*

**Remark:** if  $g''(x^*) = 0$ , the possibility of a pitchfork bifurcation can be evaluated using a normal form of higher order than the one in (3.7). However, this is out of the scope of this paper.

We now perform the centre manifold analysis for a single Hopf bifurcation.

**3.3. Single Hopf.** In the following, we employ the Taylor expansion of (1.1) with scaling about an equilibrium  $x^*$ , given by

$$\begin{aligned} y'(t) &= -Ay(t) + B(y(t-1) - e^{-A\tau}y(t-1-\tau)) + \frac{C}{2}(y^2(t-1) \\ &\quad - e^{-A\tau}y^2(t-1-\tau)) + \frac{D}{6}(y^3(t-1) - e^{-A\tau}y^3(t-1-\tau)) + O(y_t^4) \\ &= L(y(t), y(t-1), y(t-1-\tau)) + f(y(t), y(t-1), y(t-1-\tau)) + O(y_t^4), \end{aligned} \tag{3.8}$$

with  $A = \gamma\tau_1 > 0$ ,  $B = g'(x^*)\tau_1$ ,  $C = g''(x^*)\tau_1$ ,  $D = g'''(x^*)\tau_1$  and  $\tau = \tau_2/\tau_1 > 0$ .

In order to obtain the type of the Hopf bifurcation, we use the method of Campbell [8] for compute the centre manifold using the symbolic algebra package Maple. We give an overview of the different steps of computation:

- we start by computing the vector  $\mathbf{b}$  using (3.4) and the fact that for the single Hopf bifurcation we have  $\Phi = (\phi_1, \phi_2) = (\sin(\omega\theta), \cos(\omega\theta))$  ;
- we then introduce the function

$$h_2(\theta, \mathbf{z}) = h_{11}(\theta)x^2 + h_{12}(\theta)xy + h_{22}(\theta)y^2,$$

and we compute the functions  $h_{ij}$  by solving the following partial differential equation (see [8], eq. 8.31):

$$\frac{\partial h_2}{\partial \theta}(\theta, \mathbf{z}) + O(\|\mathbf{z}\|^3) = \frac{\partial h_2}{\partial \mathbf{z}}(\theta, \mathbf{z})B\mathbf{z} + \Phi(\theta)\Psi(0)\mathbf{F}_2(\Phi(\theta)\mathbf{u}) + O(\|\mathbf{z}\|^3)$$

The arbitrary constants are determined using a second partial differential equation given in [8] (eq. 8.32) ;

- the equation (3.3) becomes

$$\begin{aligned} x' &= -\omega y + b_1(f_{11}x^2 + f_{12}xy + f_{22}y^2 + f_{111}x^3 + f_{112}x^2y + f_{122}xy^2 + f_{222}y^3), \\ y' &= \omega x + b_2(f_{11}x^2 + f_{12}xy + f_{22}y^2 + f_{111}x^3 + f_{112}x^2y + f_{122}xy^2 + f_{222}y^3), \end{aligned}$$

and the type of the Hopf bifurcation is determined (see [14], eq. 3.4.11) by the sign of

$$\begin{aligned} a &= \frac{1}{8}(3b_1f_{111} + b_1f_{122} + b_2f_{112} + 3b_2f_{222}) \\ &\quad + \frac{1}{8\omega}((b_1^2 - b_2^2)f_{12}(f_{11} + f_{22}) + 2b_1b_2(f_{22}^2 - f_{11}^2)). \end{aligned} \tag{3.9}$$

The Maple commands are available online<sup>1</sup>. The final expression of  $a$  involves derivatives of  $g$  of order higher than two, such that it is not possible to compute its value without choosing a function  $g$  beforehand (see next section). Because this implies a constraint on  $B$ , the value  $a$  is computed on single points rather than on the whole stability boundary as it can be seen in [1].

In the next section, we present a detailed analysis of the bifurcations occurring at parameter values where two pairs of purely imaginary eigenvalues exist.

<sup>1</sup><http://math.univ-lyon1.fr/~pujo/platelet-regulation.html>

**4. Centre manifold analysis for double Hopf bifurcation.** In the double Hopf case, the type of the bifurcation is indicated by four coefficients  $a_{11}, a_{12}, a_{21}, a_{22}$  which are the equivalent of  $a$  in the simple Hopf case. However, there is no explicit expression of these coefficients (an equivalent to (3.9)) in the literature. Therefore they need to be computed using the symbolic algebra package Maple.

**4.1. Computing  $a_{11}, a_{12}, a_{21}, a_{22}$  using Maple.** The computation of  $a_{11}, a_{12}, a_{21}, a_{22}$  from a system of the form

$$\begin{aligned}\dot{x} &= -\omega_1 y + F_{111}^1 x^3 + F_{112}^1 x^2 y + F_{114}^1 x^2 u + F_{114}^1 x^2 v + \dots, \\ \dot{y} &= \omega_1 x + F_{111}^2 x^3 + F_{112}^2 x^2 y + F_{114}^2 x^2 u + F_{114}^2 x^2 v + \dots, \\ \dot{u} &= -\omega_2 v + F_{111}^3 x^3 + F_{112}^3 x^2 y + F_{114}^3 x^2 u + F_{114}^3 x^2 v + \dots, \\ \dot{v} &= \omega_2 u + F_{111}^4 x^3 + F_{112}^4 x^2 y + F_{114}^4 x^2 u + F_{114}^4 x^2 v + \dots,\end{aligned}\tag{4.1}$$

also written

$$\begin{pmatrix} \dot{x} \\ \dot{y} \\ \dot{u} \\ \dot{v} \end{pmatrix} = \begin{pmatrix} 0 & -\omega_1 & 0 & 0 \\ \omega_1 & 0 & 0 & 0 \\ 0 & 0 & 0 & -\omega_2 \\ 0 & 0 & \omega_2 & 0 \end{pmatrix} \begin{pmatrix} x \\ y \\ u \\ v \end{pmatrix} + \begin{pmatrix} f_1(x, y, u, v) \\ f_2(x, y, u, v) \\ f_3(x, y, u, v) \\ f_4(x, y, u, v) \end{pmatrix},\tag{4.2}$$

of a double Hopf bifurcation follows the steps explained by Guckenheimer [14] in the ‘‘appendix to Section 3.4’’. It relies on writing (4.2) as a complex system, that is

$$\begin{aligned}\dot{z}_1 &= \lambda_1 z_1 + h(z_1, \bar{z}_1, z_2, \bar{z}_2), \\ \dot{z}_2 &= \lambda_2 z_2 + g(z_1, \bar{z}_1, z_2, \bar{z}_2),\end{aligned}\tag{4.3}$$

with  $\lambda_i = i\omega_i$ ,  $z_1 = x + iy$ ,  $z_2 = u + iv$ , and writing the normal form for the double Hopf as a complex system, that is

$$\begin{aligned}w_1' &= \lambda_1 w_1 + c_{11} w_1^2 \bar{w}_1 + c_{12} w_1 \bar{w}_2 w_2 + O(|w_1, w_2|^5) =: \lambda_1 w_1 + \hat{h}_1(w_1, \bar{w}_1, w_2, \bar{w}_2), \\ w_2' &= \lambda_2 w_2 + c_{21} w_1 \bar{w}_1 w_2 + c_{22} w_2^2 \bar{w}_2 + O(|w_1, w_2|^5) =: \lambda_2 w_2 + \hat{h}_2(w_1, \bar{w}_1, w_2, \bar{w}_2).\end{aligned}\tag{4.4}$$

To transform (4.3) to (4.4), we use the near identity transformation

$$\begin{aligned}z_1 &= w_1 + \Psi(w_1, \bar{w}_1, w_2, \bar{w}_2), & \Psi &= O(|w_1, w_2|^2), \\ z_2 &= w_2 + \Phi(w_1, \bar{w}_1, w_2, \bar{w}_2), & \Phi &= O(|w_1, w_2|^2).\end{aligned}\tag{4.5}$$

Substituting (4.5) in (4.3) and using (4.4), we obtain two partial differential equations *PDE1* and *PDE2* (see the file BP-MB 2018 - computations double Hopf.mw online<sup>2</sup>).

We give an overview of the different steps of computation performed in Maple :

- We introduce the Taylor expansion to the second order of  $\Phi, \Psi, h, g$ , that we substitute in *PDE1* and *PDE2*. Equating coefficients of  $w_i, w_j, w_i \bar{w}_j$  and  $\bar{w}_i \bar{w}_j$  we obtain expressions of the partial derivatives of  $\Phi, \Psi$  as functions of partial derivatives of  $h, g$ .
- We introduce the Taylor expansion to the third order of  $h, g$  that we substitute in *PDE1* and *PDE2*. Equating coefficients of  $w_1^2 \bar{w}_1, w_1 \bar{w}_2 w_2, w_1 \bar{w}_1 w_2$  and  $w_2^2 \bar{w}_2$ , we obtain expressions of the coefficients  $c_{11}, c_{12}, c_{21}, c_{22}$  as functions of the partial derivatives of  $h, g$ . The coefficients of interest  $a_{11}, a_{12}, a_{21}, a_{22}$  are given as  $a_{ij} = \text{Re}(c_{ij})$ .

<sup>2</sup><http://math.univ-lyon1.fr/~pujo/platelet-regulation.html>

- To obtain expressions of the partial derivatives of  $h, g$  as functions of the partial derivatives of  $f_i, i = 1, 2, 3, 4$ , we use the Taylor expansion to the third order of  $f_i, i = 1, 2, 3, 4$  and the fact that  $h = f_1 + if_2, g = f_3 + if_4$ .
- The partial derivatives of  $f_i, i = 1, 2, 3, 4$  are computed as functions of the  $F_{ijk}^l, i, j, k, l = 1, 2, 3, 4$  of (4.1).

From there, the computation of the  $F_{ijk}^l, i, j, k, l = 1, 2, 3, 4$  of (4.1) is performed following the adaptation of the method of Campbell [8] used in Section 3.3 to the case of double Hopf bifurcation. The Maple commands are available online<sup>3</sup>.

**4.2. Calculating the centre manifold of the double Hopf bifurcation.** In the case of the double Hopf bifurcation, there are two values of  $\omega$  satisfying (2.5) for the same values of  $A, B$  and  $\tau$ :

$$\begin{aligned} A &= +B[\cos \omega_1 - e^{-A\tau} \cos(\omega_1(1 + \tau))], \\ \omega_1 &= B[-\sin \omega_1 + e^{-A\tau} \sin(\omega_1(1 + \tau))], \\ 0 &= A + B[\cos \omega_2 - e^{-A\tau} \cos(\omega_2(1 + \tau))], \\ \omega_2 &= B[-\sin \omega_2 + e^{-A\tau} \sin(\omega_2(1 + \tau))]. \end{aligned}$$

And the elements needed to write (3.3) are

$$\Phi = (\phi_1, \phi_2, \phi_3, \phi_4) = (\sin(\omega_1\theta), \cos(\omega_1\theta), \sin(\omega_2\theta), \cos(\omega_2\theta)), \quad \mathbf{z} = (x, y, u, v)^T, \quad (4.6)$$

such that  $\Phi \mathbf{z} = \sin(\omega_1\theta)x + \cos(\omega_1\theta)y + \sin(\omega_2\theta)u + \cos(\omega_2\theta)v$ ,

$$B = \begin{bmatrix} 0 & -\omega_1 & 0 & 0 \\ \omega_1 & 0 & 0 & 0 \\ 0 & 0 & 0 & -\omega_2 \\ 0 & 0 & \omega_2 & 0 \end{bmatrix}, \quad \text{and } \mathbf{b} = \begin{pmatrix} K_{12}, \\ K_{22}, \\ K_{34}, \\ K_{44} \end{pmatrix},$$

$$\text{with } K = \begin{bmatrix} \frac{\langle \Phi_{12}^T, \Phi_{12} \rangle^T}{D_{12}^2} & 0 \\ 0 & \frac{\langle \Phi_{34}^T, \Phi_{34} \rangle^T}{D_{34}^2} \end{bmatrix}, \quad D_{ij}^2 = \det \langle \Phi_{12}^T, \Phi_{12} \rangle \text{ and } \Phi_{ij} = (\phi_i, \phi_j).$$

In order to obtain the type of the Hopf bifurcation, we use the method of Campbell [8] for calculating centre manifold using the symbolic algebra package Maple. The algorithm using Maple and its results are available online<sup>4</sup>. For sake of clarity, we decide to only give an overview of the different steps of computation to them:

- we start by computing the vector  $\mathbf{b}$  using (3.4);
- we then introduce the function

$$\begin{aligned} h_2(\theta, \mathbf{z}) &= h_{11}(\theta)x^2 + h_{12}(\theta)xy + h_{13}(\theta)xu + h_{14}(\theta)xv + h_{22}(\theta)y^2 \\ &\quad + h_{23}(\theta)yu + h_{24}(\theta)yv + h_{33}(\theta)u^2 + h_{34}(\theta)uv + h_{44}(\theta)v^2 \end{aligned}$$

and we compute the functions  $h_{ii}$  by solving the following partial differential equation (see [8], equation 8.31):

$$\frac{\partial h_2}{\partial \theta} + O(\|\mathbf{z}\|^3) = \frac{\partial h_2}{\partial \mathbf{z}}(\theta, \mathbf{z})B\mathbf{z} + \Phi(\theta)\Psi(0)\mathbf{F}_2(\Phi(\theta)\mathbf{u}) + O(\|\mathbf{z}\|^3)$$

The arbitrary constants are determined using a second partial differential equation (see [8], equation 8.32);

<sup>3</sup><http://math.univ-lyon1.fr/~pujo/platelet-regulation.html>

<sup>4</sup><http://math.univ-lyon1.fr/~pujo/platelet-regulation.html>

- we then obtain the equation (3.3) under the form (4.1).

Combining with the expressions of  $a_{11}, a_{12}, a_{21}, a_{22}$  as functions of the coefficients of (4.1), we have an expression of  $a_{11}, a_{12}, a_{21}, a_{22}$  as a function of  $A, B, C, D, \omega$  and  $\tau$ . The Maple commands are available online<sup>5</sup>.

**4.3. From the values of  $a_{11}, a_{12}, a_{21}, a_{22}$  to the descriptions of the flows near the double Hopf.** We introduce the continuous functions  $\mu_1, \mu_2, \Omega_1, \Omega_2$  on  $\mathbb{R}_+^2$  describing the branches of eigenvalues associated with the purely imaginary eigenvalues  $\omega_1$  and  $\omega_2$ , *i.e.* such that for a point  $(\tau, B)$ ,

$$\lambda_{1\pm}(\tau, B) = \mu_1(\tau, B) \pm i\Omega_1(\tau, B), \quad \text{and } \lambda_{2\pm}(\tau, B) = \mu_2(\tau, B) \pm i\Omega_2(\tau, B)$$

are two pairs of simple complex-conjugate eigenvalues such that  $\lambda_{1+}(\tau_0, B_0) = i\omega_1$  and  $\lambda_{2+}(\tau_0, B_0) = i\omega_2$ . According to the theory of centre manifold analysis, if  $(\tau_1, B_1)$  is a point close to  $(\tau_0, B_0)$ , then System (4.1) is approximated by a system in radial components given by

$$\begin{aligned} \dot{r}_1 &= \mu_1(\tau_1, B_1)r_1 + a_{11}r_1^3 + a_{12}r_1r_2^2, \\ \dot{r}_2 &= \mu_2(\tau_1, B_1)r_2 + a_{21}r_1^2r_2 + a_{22}r_2^3, \\ \dot{\theta}_1 &= \omega_1(\tau_1, B_1), \\ \dot{\theta}_2 &= \omega_2(\tau_1, B_1), \end{aligned} \tag{4.7}$$

and the possible dynamics are explored by studying the ‘‘amplitude system’’ for  $r_1, r_2 \geq 0$  given by

$$\begin{aligned} \dot{r}_1 &= \mu_1(\tau_1, B_1)r_1 + a_{11}r_1^3 + a_{12}r_1r_2^2, \\ \dot{r}_2 &= \mu_2(\tau_1, B_1)r_2 + a_{21}r_1^2r_2 + a_{22}r_2^3. \end{aligned} \tag{4.8}$$

Indeed, equivalences have been established [17] between the positions of the equilibria of (4.8) and the dynamics of the solutions of (4.7):

- an equilibrium at  $r_1 = r_2 = 0$  for (4.8) corresponds to an equilibrium point at the origin for (4.7) ;
- a non-trivial equilibrium on one of the axis for (4.8) corresponds to cycle for (4.7) ;
- an equilibrium with  $r_1, r_2 > 0$  for (4.8) corresponds to two-dimensional torus for (4.7) ;
- a limit cycle for (4.8) corresponds to three-dimensional torus for (4.7).

We find in Kuznetsov ([17], Section 8.6.2) a description of all the possible subcases (called the ‘‘unfolding’’ of (4.8)), depending on the signs of  $a_{11}a_{22}$ ,  $\theta := \frac{a_{12}}{a_{22}}$ ,  $\delta := \frac{a_{21}}{a_{11}}$  and  $\theta\delta - 1$ .

**4.4. Application to the equation  $x'(t) = -\gamma x(t) + g(x(t - \tau_1)) + g(x(t - \tau_1 - \tau_2))e^{-\gamma\tau_2}$ .** We go back to the bifurcation regions of, and focus on the double Hopf bifurcation happening when the stability boundary of  $B < 0$  crosses itself. As said before, a change in stability occurs through a Hopf bifurcation only if  $B < 0$ , and we see that there exist  $\omega_1, \omega_2$  such that  $(\tau(\omega_1), B(\omega_1)) = (\tau(\omega_2), B(\omega_2)) = (\tau_0, B_0)$  with  $B_0 = -1.6006 < 0$  and  $\tau_0 = 4.1693$  (see Figure 2.2).

Because the expressions of  $a_{ij}$  involve  $C$  and  $D$ , we need to fix  $g$  such that the point  $(\tau, B)$  corresponds to the crossing of the lower stability boundary seen

<sup>5</sup><http://math.univ-lyon1.fr/~pujo/platelet-regulation.html>

on Figure 2.2 : we choose  $g(x) := f_0 \frac{\sigma^n}{\sigma^n + x^n} + \beta_0$  with  $f_0 = 5 \times 10^{10}$ ,  $\beta_0 = 0.01$ ,  $\sigma = 8 \times 10^9$  and  $n = 10.166$ . In this case, and assuming that the curve decreases with  $\tau$  corresponds to  $\omega_1$ , we have

$$\begin{aligned} a_{11} > 0, \quad a_{12} > 0, \quad a_{21} < 0, \quad a_{22} < 0, \\ \theta := \frac{a_{12}}{a_{22}} < 0, \quad \delta := \frac{a_{21}}{a_{11}} < 0, \quad \theta\delta - 1 > 0, \end{aligned} \quad (4.9)$$

which corresponds to subcase VI of the “complex” case in Kuznetsov numbering scheme (see [17] p. 363). The Maple commands are available online<sup>6</sup>.

Figure 4.1 represents the different phase portraits for the system (4.8) associated with different sectors of the  $(\mu_1, \mu_2)$  plane. We recall that given the definitions of

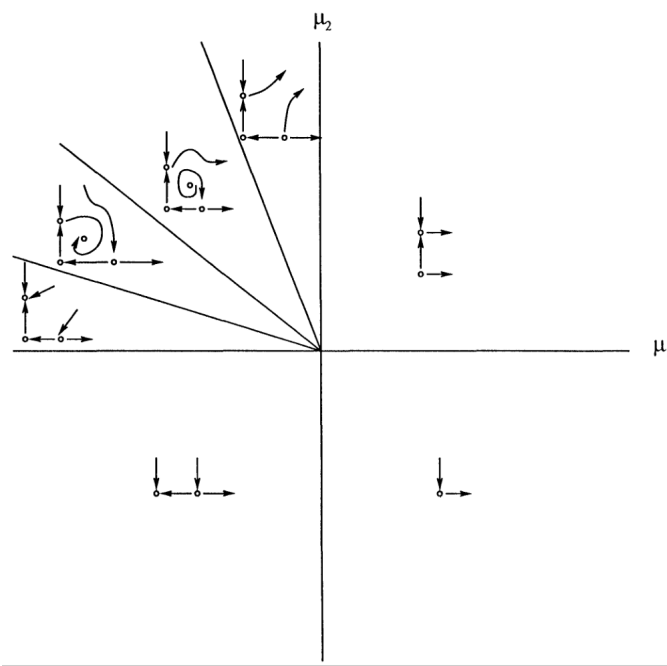


FIGURE 4.1. Parametric portraits for the phase portraits near the double Hopf bifurcation (from [1], Figure 3.3).

$\mu_1$  and  $\mu_2$ , we have  $\mu_1 > 0$  under the curve of Figure 2.2 which decreases with  $\tau$  near the double bifurcation, while  $\mu_2 < 0$  and  $\mu_2 > 0$  respectively above and under the curve of Figure 2.2 which increases with  $\tau$  near the double bifurcation. Using the relations between (4.8) and (4.7) given above, parameters corresponding to the lowest wedge of the  $\mu_1 < 0, \mu_2 > 0$  quadrant of Figure 4.1 should imply a stable limit cycle, while parameters corresponding to the lowest interior wedge of the  $\mu_1 < 0, \mu_2 > 0$  quadrant of Figure 4.1 should imply a stable torus.

**4.5. Simulations.** We give two examples of simulations depicting such behaviors in Figures 4.2 and 4.3, for the case where  $g$  and its parameters are as defined in the previous subsection.

<sup>6</sup><http://math.univ-lyon1.fr/~pujo/platelet-regulation.html>

For Figure 4.2, we have  $n = 11$ ,  $\tau_2 = 4.75 \times \tau_1$ , and the corresponding eigenvalues have real parts  $\mu_1 = -0.0651$ ,  $\mu_2 = 0.0014$ , such that  $\mu_2 < \mu_1/\theta = 0.1023$ . This implies that it is under the line  $T_1$  defined by Kuznetsov [17], such that this point corresponds to the lowest wedge of the  $\mu_1 < 0, \mu_2 > 0$  quadrant of Figure 4.1. And as predicted by the unfolding, the solution converges to a stable limit cycle.

For Figure 4.3, we have  $n = 11$ ,  $\tau_2 = 4.24 \times \tau_1$ , and the corresponding eigenvalues have real parts  $\mu_1 = -0.0078$ ,  $\mu_2 = 0.0188$ , such that  $\mu_2 > \mu_1/\theta = 0.0123$  and  $\mu_2 < -\frac{\delta-1}{\theta-1}\mu_1 = 0.0334$ . This implies that it is above the line  $T_1$  and under the line  $C$  defined by Kuznetsov [17], such that this point corresponds to the lowest interior wedge of the  $\mu_1 < 0, \mu_2 > 0$  quadrant of Figure 4.1. As predicted by the unfolding, the solution converges to a torus.

For Figure 4.4, we have  $n = 11$ ,  $\tau_2 = \times \tau_1$ , and this point corresponds to the  $\mu_1 > 0, \mu_2 > 0$  quadrant of Figure 4.1. The unfolding cannot be used to predict the behaviour of the solution, and we see that a stable cycle appears.

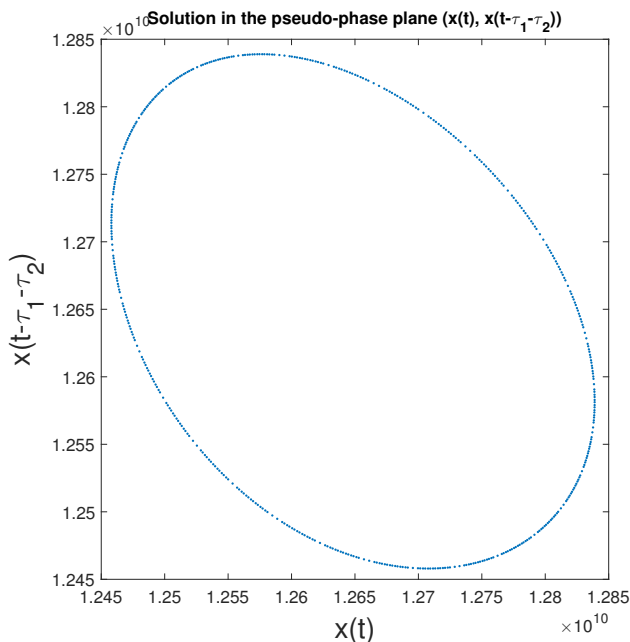


FIGURE 4.2. Numerical simulation of (1.1) for  $\tau_2 = 4.75 \times \tau_1$  in the pseudo-phase plane  $(x(t), x(t - \tau_1 - \tau_2))$ , corresponding to the lowest wedge of the  $\mu_1 < 0, \mu_2 > 0$  quadrant of Figure 4.1. Once the transient dynamic is lost, a stable limit cycle appears.

In the next section, we use the computation presented in Section 3.3 to determine the criticality of Hopf bifurcation for a model of platelet production.

**5. Application to the production of platelets.** As mentioned in the introduction, we now use the results obtained above on a model describing the production of platelets, in order to study the role of the two mechanisms for destruction (random and deterministic). This model may be seen as a simplification of the one given in

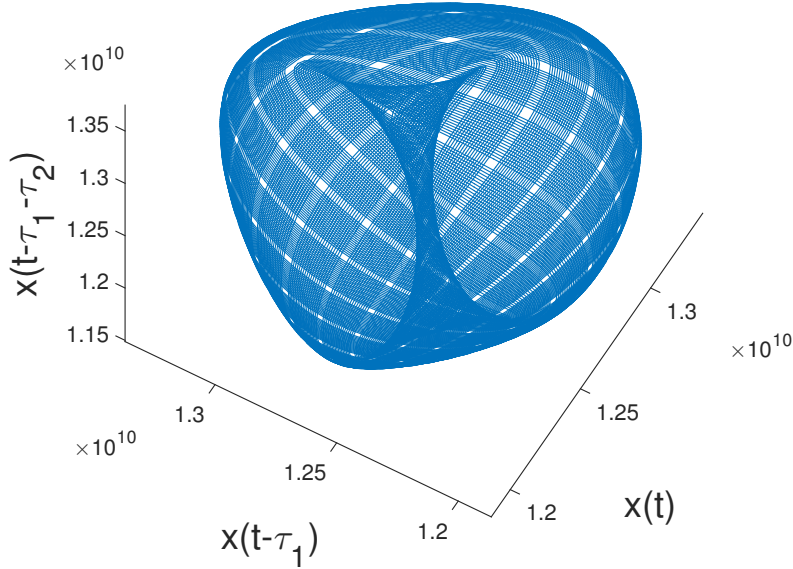


FIGURE 4.3. Numerical simulation of (1.1) for  $\tau_2 = 4.24 \times \tau_1$  in the pseudo-phase space  $(x(t), x(t - \tau_1), x(t - \tau_1 - \tau_2))$ , corresponding to the lowest interior wedge of the  $\mu_1 < 0, \mu_2 > 0$  quadrant of Figure 4.1. Once the transient dynamic is lost, a stable torus appears.

[6]. Indeed, we represent the regulation by the platelet number not as a continuous action on the maturity speed of megakaryocyte progenitors, but more directly by a regulation of the rate of production of new megakaryocytes. In order to reproduce the fact that this production rate is bounded below and above, we express it as a function of the platelet count  $G(P) = \bar{m} \frac{\sigma^n}{\sigma^n + P^n} + \underline{m}$ . We consider that  $\tau_1$  is the time between the birth of a megakaryocyte and the time its cytoplasm sheds into platelets. Furthermore we assume that platelets die randomly with a rate  $\gamma$  and are removed from the system by macrophages and hepatocytes after a survival time  $\tau_2$  [12, 19]. Then the model is described by the following equation:

$$x'(t) = -\gamma x(t) + g(x(t - \tau_1)) - g(x(t - \tau_1 - \tau_2))e^{-\gamma\tau_2}, \quad (5.1)$$

with  $g(P) = A_0 G(P) = f_0 \frac{\sigma^n}{\sigma^n + P^n} + \beta_0$ ,  $A_0$  the number of platelet per megakaryocyte.

**5.1. Parameter estimates.** Based on observations of a delay of 5 days between stimulation by thrombopoietin and a rise in platelet count [16], we choose  $\tau_1 = 5$ ; and we set  $\tau_2 = 8.4$  using observed mean platelet survival time [27]. Furthermore, the following biological observations allow us to obtain  $f_0$ ,  $\beta_0$  and  $\sigma$ :

- at steady state, the amount of platelets is  $x^* = 20 \times 10^9/\text{kg}$  [23], such that

$$-\gamma x^* + f_0 \left( \frac{\sigma^n}{\sigma^n + x^{*n}} + \beta_0 \right) (1 - e^{-\gamma\tau_2}) = 0;$$

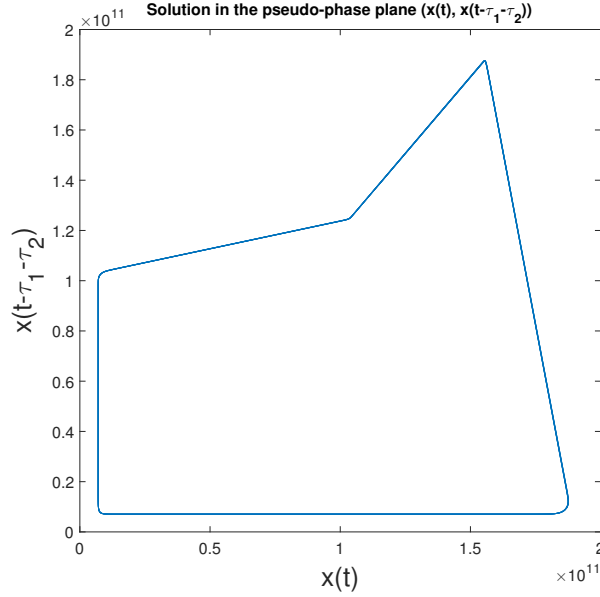


FIGURE 4.4. Numerical simulation of (1.1) for  $\tau_2 = 4.24 \times \tau_1$  in the pseudo-phase plane  $(x(t), x(t - \tau_1 - \tau_2))$ , corresponding to the  $\mu_1 > 0, \mu_2 > 0$  quadrant of Figure 4.1. Once the transient dynamic is lost, a stable limit cycle appears.

- when the feedback is deactivated, which for the regulation system is equivalent to a virtually infinite amount of platelets, the amount of platelets is divided by 10 [9], such that

$$-\gamma x^*/10 + f_0 \beta_0 (1 - e^{-\gamma \tau_2}) = 0;$$

- the maximum increase reached with an artificial simulation of the hormone signal controlling platelet production, equivalent to a population of 0, leads to an 10-fold increase [15], such that

$$-\gamma x^* \times 10 + f_0 (1 + \beta_0) (1 - e^{-\gamma \tau_2}) = 0.$$

Therefore, only the parameters  $\gamma$  and  $n$  are not determined by the model. Until appropriate data is available, we decide to use Langlois *et al.* fitted value of  $\gamma = 0.05$  [18]. Finally, we choose  $n = 1.7$  such that the unique equilibrium is stable when parameters correspond to healthy patients (that is,  $\tau_2 = 8.4$  and  $\gamma = 0.05$ ).

**5.2. Stability analysis.** As  $g$  is decreasing, we are interested in the part of the  $(B, \tau)$  plane corresponding to  $B \leq 0$ . We study the effect of increasing platelet death rate, that is, increasing  $\gamma$ ; and of decreasing the platelet survival time, that is, decreasing  $\tau_2$ . Plots of the evolution of  $B = f_0 g'(x^*) \tau_1$  as either  $\gamma$  increases or as  $\tau_2$  decreases are given in Figure 5.1. We see that when  $\tau_2$  decreases of one day (to  $\tau_2 = 7.2$ ), then the system loses its stability. Furthermore, if  $\gamma$  is 10-fold then the system also loses its stability.

Numerical solutions for (1.1) are shown on Figure 5.2 for  $(\tau_2, \delta)$  pairs associated with the different stability regions seen on Figure 5.1. We notice that both  $\gamma$  and  $\tau_2$  can lead to a change in stability if modified: when the curve  $B(\omega)$  leaves the

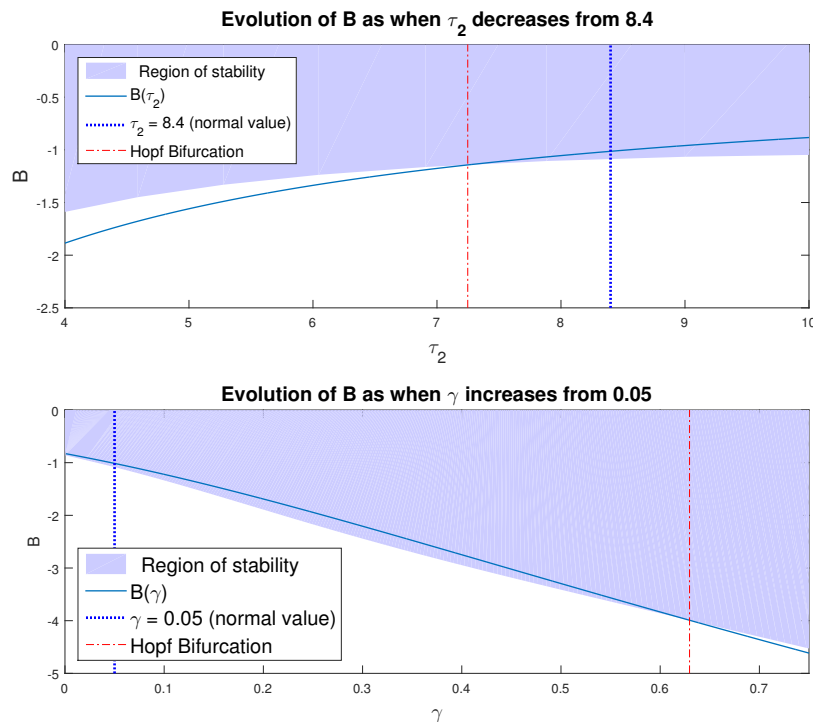


FIGURE 5.1. Stability as  $\tau_2$  or  $\gamma$  are varied and other parameters are fixed. Blue dotted lines represent the values in healthy patients, and red dotted lines mark the limits after which the equilibrium is unstable. We see that when  $\tau_2$  decreases of one day (to  $\tau_2 = 7.2$ ), then the system loses its stability. Furthermore, if  $\gamma$  is multiplied more than 12 times (to  $\gamma = 0.625$ ) then the system also loses its stability.

zone of stability, a Hopf bifurcation occurs. Furthermore, the criticality of the Hopf bifurcation is computed in both cases using the expression (3.9) of  $a$  computed in Maple (see online<sup>7</sup>). In both cases,  $a$  is negative such that the bifurcation is supercritical and a locally stable periodic solution appears, as seen on the solutions obtained numerically.

Other characteristics of the dynamics change differently depending on the bifurcation parameter: the main consequence of decreasing  $\tau_2$  is an increase in amplitude, but increasing  $\gamma$  decreases the overall value of platelet count. However, from a clinical point of view a decrease in platelet survival time  $\tau_2$  seems to induce a more threatening chronic thrombocytopenia than a change in  $\gamma$ , as well as inducing a chronic thrombocytosis.

**6. Conclusion.** In an attempt to model the quantity of platelets in the blood as affected by both a random and an age-related destruction, we analyze a delay

<sup>7</sup><http://math.univ-lyon1.fr/~pujo/platelet-regulation.html>

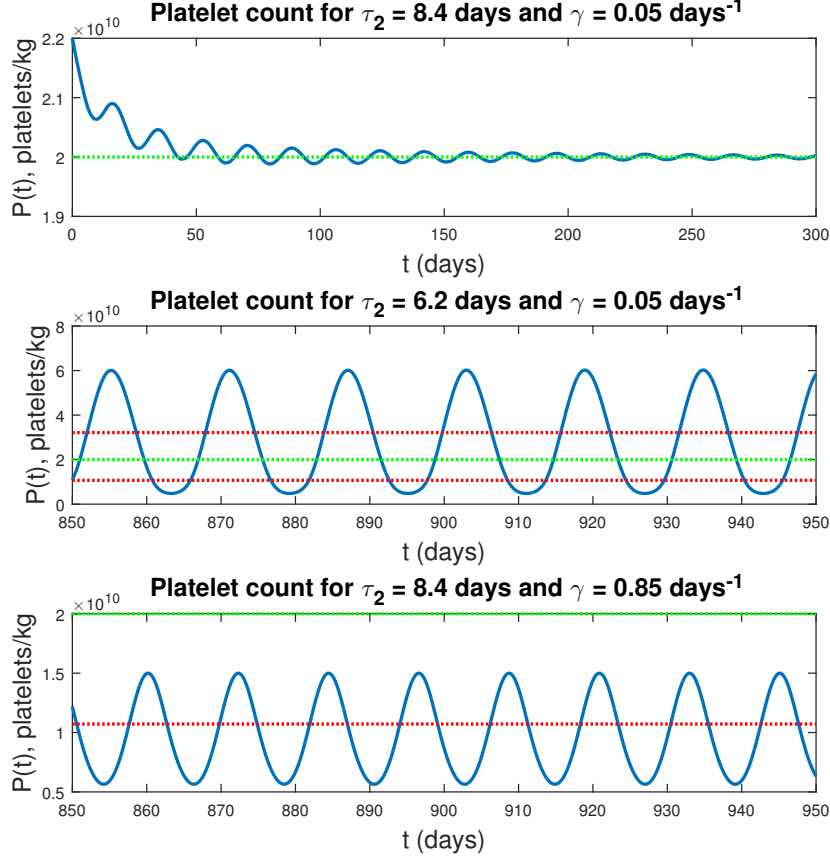


FIGURE 5.2. The evolution of the platelet count with time (blue line) for different values of  $\tau_2$  and  $\gamma$ , after the transient phase. The green dotted line represents the average platelet count of healthy patients,  $20 \times 10^9$  platelets/kg, and the two red dotted lines represent the healthy range of platelet count,  $11 \times 10^9 - 32 \times 10^9$ .

differential equation with two delays presented by Bélair *et al.* in 1987 [2]. In order to complete the already existing body of work dedicated to two-delays differential equations, we studied the stability of the equilibrium points for a scaled linearized version of the equation described by three parameters,  $A$ ,  $B$  and  $\tau$ . As the purely imaginary eigenvalues can not be identified analytically, we used a numerical method, D-decomposition, to obtain curves in the plans  $(\tau, B)$  and  $(A, B)$  corresponding to the existence of a pair of purely imaginary eigenvalues. Associated with a study of the transversality condition in  $A$  then in  $\tau$ , we obtain the number of eigenvalues with positive real parts in the different stability regions. This analysis is then completed with a centre manifold analysis for the steady-state bifurcation, as well as for the single Hopf bifurcation, allowing us to test whether leaving the

region of stability through a Hopf bifurcation is associated with the onset of periodic solutions. Furthermore, the existence of self-intersection in the stability boundary associated with Hopf bifurcation revealed the possibility of a double Hopf bifurcation, a phenomenon known to generate a variety of complex dynamical behaviors. Therefore we performed a centre manifold analysis near the point where a double bifurcation occurs, revealing the possibility of torus-like dynamics near the region where two eigenvalues with positive real parts exist.

Finally, coming back to the model for platelet production, we use the results on the single Hopf bifurcation to explore the impact of an increase in death rate or a decrease in survival time on the onset of periodic dynamics, as we expected from the platelet-specific antibodies observed in patients with cyclic thrombocytopenia. We choose a megakaryocyte production rate which decreases when the platelet count increases, while always staying strictly positive and finite. The parameters of this feedback function are identified using the normal mean platelet count as an equilibrium. Finally, we show that although stability is gained by going from left to right in the plane  $(B, \gamma)$ , taking in account the role of  $\gamma$  in the computation of  $B = g'(x^*)\tau_1$  enables to lose stability when increasing the death rate  $\gamma$  of platelets. The same counter-intuitive conclusion is obtained for a decrease of the survival time of platelets  $\tau_2$ . The extent of the change in  $\tau_2$  necessary to induce oscillations seems more reasonable than that of  $\gamma$ . In the cases of cyclic thrombocytopenia of the auto-immune type, platelet-specific antibodies are observed in patients blood. Therefore, our work indicates that auto-immune cyclic thrombocytopenia is more likely to be due to a over-reactive system of old platelet removal, rather than to an increase random destruction of platelets of any age. However, this relies on the likelihood of a small decrease of  $\tau_2$  being more important than the likelihood of a important increase of  $\gamma$ , which needs to be confirmed with clinicians.

Notice that although regularities appear in the graphs of the stability curve, such as an ordering in the curves corresponding to different intervals  $[\pi + 2n\pi, 2(n + 1)\pi], n \in \mathbb{N}$  or a equivalence between the transversality condition and the concavity of the function  $B \mapsto B(\omega)$ , we were not able to obtain an analytical proof for such results. Besides, we encountered difficulties in simulating the solutions of (1.1) corresponding the sections 1, 2 and 6 of the unfolding (Figure 4.1). These questions are still open and will be the object of a future work.

Most works on the stability of two-delays differential equations focus on a limited version of (1.3). For example, Bélair & Campbell [1] studied the case where  $A = 0$  and  $B = 1$ , and focused on the features of the stable regions in the plane  $(A, r_2)$  as  $r_1$  increases. In particular, authors obtained intersecting stability curves associated with a double Hopf bifurcation. Using centre manifold analysis, they identified two sets of parameters such that near the double Hopf bifurcation, the unfolding corresponds to type Ib of Guckenheimer & Holmes [14] for one, and VIa for the other (which corresponds to the subcase VI of the “complex” case in Kuznetsov numbering scheme (see [17] p. 363)). The authors were also able to show that when  $r_1$  increases, the stability region becomes composed of disconnected stable regions, a feature previously thought to be impossible. Interestingly, while the choice of fixing  $A$  to 0 simplifies the computation of the stability regions, the identification of bifurcation type still relies on numerical methods. Using a normalization such that  $r_1 = 1$ , Mahaffy *et al.* [21] focused on the stability regions in the 3D-space  $(A, B, C)$ . Indeed, once  $A$  and  $r_2$  are fixed, the computation of the values of  $B$  and  $C$  corresponding to the existence of a pair of purely imaginary eigenvalues

is straightforward. In particular, the authors identified regions in the plane  $(R, A)$  corresponding to different configurations of the stability regions in the plane  $(B, C)$ , and noticed that there exists two disconnected regions for  $A < 0$ . Mahaffy & Busken [7] returned later to the study of the stability regions in the plane  $(B, C)$  while this time focusing on the differences observed between the case  $r_2 \in \mathbb{Q}$  and  $r_2 \notin \mathbb{Q}$ . Finally, Besse [4] analyzed the stability of (1.3) by presenting the stability regions for  $C < 0$ ,  $r_1$  and  $r_2$  fixed. The author introduced a change of variable  $x = A + B$  and  $y = -A + B$ , such that the stability for  $x < -C$  or for  $y < C$  is straightforward. The stability for  $y \geq C, x \geq -C$ , however, is non-trivial, as for high  $r_2$  it involves intertwined loops. The author were nevertheless able to obtain a region of the plane  $(x, y)$  in which the system is stable for any  $r_2 \geq 0$ , at the condition  $C \geq -\pi/r_1$ . In our case, a change of stability occurs once along an increase of a parameter of the model. However, it is known that such a change in stability is sometimes reversed by increasing the parameter further. This is often the case when the coefficients of the characteristic equation involve the delay, as in [24, 25]. In our case, the coefficients do not involve the delays, and for the application that we study, we do not have stability switches. However, it is not impossible that given different parameters or functions our model would present stability switches as the use of two delays implies an increase in complexity such that delay-dependent coefficients are not needed for stability switches. For example, disconnected stability regions have been observed for such models by Bélair and Campbell [1], which is a feature conducive to stability switches.

Although most of the aforementioned papers rely on the method of D-decomposition, they do not use it to study the effect of parameters changes as we did in Section 5. Therefore we mention two papers dedicated to models of erythropoiesis (the production of red blood cells) applying it. In the first one, Bélair *et al.* [3] studies the stability of the equilibrium of a system of two differential equations with two delays, and the analysis relies on a characteristic equation given by

$$(\lambda + \gamma)(\lambda + k) = -A(e^{-\lambda T_1} - e^{-\gamma T_1} e^{-\lambda(T_1+T_2)}),$$

where  $A$  depends on the steady state. It is a more complicated version of (1.3) with an additional  $\lambda^2$ . Authors identify numerically the stability region in the plane  $(\gamma, A)$ , and similarly to the conclusion presented in Section 5, stability is gained when one moves from left to right in the plane  $(A, \gamma)$  but the role of  $\gamma$  in the computation of  $A$  implies that increasing  $\gamma$  can lead to instability. A similar phenomenon was obtained later by Mahaffy *et al.* [20] in a second paper on a model of erythropoiesis with a state-dependent delay.

Finally, we notice that equation (1.1) can also be obtained by adding a survival time for platelets to a model of megakaryopoiesis whose stability was recently analyzed [5]. In the case of this model, we have  $\tau_1 > \tau_2$ , which according to preliminary numerical explorations (not shown) seems to imply that stability is not affected of the value of  $\gamma$ .

## REFERENCES

- [1] J. Bélair and S. A. Campbell, Stability and Bifurcations of Equilibria in a Multiple-Delayed Differential Equation, *SIAM Journal on Applied Mathematics*, **54** (1994), 1402–1424.
- [2] J. Bélair and M. C. Mackey, A Model for the Regulation of Mammalian Platelet Production, *Annals of the New York Academy of Sciences*, **504** (1987), 280–282.
- [3] J. Bélair, M. C. Mackey and J. M. Mahaffy, Age-structured and two delay models for erythropoiesis, *Math. Biosciences*, **128** (1995), 317–346.

- [4] A. Besse, *Modélisation Mathématique de La Leucémie Myéloïde Chronique*, Ph.D thesis, Université Claude Bernard Lyon 1, 2017.
- [5] L. Boullu, M. Adimy, F. Crauste and L. Pujo-Menjouet, Oscillations and Asymptotic Convergence for a Delay Differential Equation Modeling Platelet Production, *Discrete and Continuous Dynamical Systems Series B*, **24** (2019), 2417–2442.
- [6] L. Boullu, L. Pujo-Menjouet and J. Wu, A model for megakaryopoiesis with state-dependent delay, *submitted*.
- [7] T. C. Busken and J. M. Mahaffy, Regions of stability for a linear differential equation with two rationally dependent delays, *Discrete and Continuous Dynamical Systems*, **35** (2015), 4955–4986.
- [8] S. A. Campbell, Calculating Centre Manifolds for Delay Differential Equations Using Maple, in *Delay Differential Equations*, Springer US, 2009, 1–24.
- [9] F. J. de Sauvage, K. Carver-Moore, S. M. Luoh, A. Ryan, M. Dowd, D. L. Eaton and M. W. Moore, Physiological regulation of early and late stages of megakaryocytopoiesis by thrombopoietin, *The Journal of Experimental Medicine*, **183** (1996), 651–656.
- [10] H. A. El-Morshedy, G. Rst and A. Ruiz-Herrera, Global dynamics of delay recruitment models with maximized lifespan, *Zeitschrift für angewandte Mathematik und Physik*, **67** (2016).
- [11] R. S. Go, Idiopathic cyclic thrombocytopenia, *Blood Reviews*, **19** (2005), 53–59.
- [12] R. Grozovsky, A. J. Begonja, K. Liu, G. Visner, J. H. Hartwig, H. Falet and K. M. Hoffmeister, The Ashwell-Morell receptor regulates hepatic thrombopoietin production via JAK2-STAT3 signaling, *Nature Medicine*, **21** (2015), 47–54.
- [13] E. N. Gryazina, The D-Decomposition Theory, *Automation and Remote Control*, **65** (2004), 1872–1884.
- [14] J. Guckenheimer and P. Holmes, *Nonlinear Oscillations, Dynamical Systems, and Bifurcations of Vector Fields*, vol. 42 of Applied Mathematical Sciences, Springer New York, 1983.
- [15] K. Kaushansky, Megakaryopoiesis and Thrombopoiesis, in *Williams Hematology*, 9th edition, McGraw-Hill, 2016, 1815–1828.
- [16] D. J. Kuter, The biology of thrombopoietin and thrombopoietin receptor agonists, *International Journal of Hematology*, **98** (2013), 10–23.
- [17] Y. A. Kuznetsov, *Elements of Applied Bifurcation Theory*, 2nd edition, no. 112 in Applied mathematical sciences, Springer, 1998.
- [18] G. P. Langlois, M. Craig, A. R. Humphries, M. C. Mackey, J. M. Mahaffy, J. Belair, T. Moulin, S. R. Sinclair and L. Wang, Normal and pathological dynamics of platelets in humans, *Journal of Mathematical Biology*, **75** (2017), 1411–1462.
- [19] J. Li, D. E. van der Wal, G. Zhu, M. Xu, I. Yougbare, L. Ma, B. Vadasz, N. Carrim, R. Grozovsky, M. Ruan, L. Zhu, Q. Zeng, L. Tao, Z.-m. Zhai, J. Peng, M. Hou, V. Leytin, J. Freedman, K. M. Hoffmeister and H. Ni, Desialylation is a mechanism of Fc-independent platelet clearance and a therapeutic target in immune thrombocytopenia, *Nature Communications*, **6** (2015).
- [20] J. M. Mahaffy, J. Bélair and M. C. Mackey, Hematopoietic Model with Moving Boundary Condition and State Dependent Delay: Applications in Erythropoiesis, *Journal of Theoretical Biology*, **190** (1998), 135–146.
- [21] J. M. Mahaffy, K. M. Joiner and P. J. Zak, A geometric analysis of stability regions for a linear differential equation with two delays, *International Journal of Bifurcation and Chaos*, **05** (1995), 779–796.
- [22] S. E. McKenzie, S. M. Taylor, P. Malladi, H. Yuhan, D. L. Cassel, P. Chien, E. Schwartz, A. D. Schreiber, S. Surrey and M. P. Reilly, The Role of the Human Fc Receptor FcγRIIA in the Immune Clearance of Platelets: A Transgenic Mouse Model, *The Journal of Immunology*, **162** (1999), 4311–4318.
- [23] L. Pitcher, K. Taylor, J. Nichol, D. Selsi, R. Rodwell, J. Marty, D. Taylor, S. Wright, D. Moore, C. Kelly and A. Rentoul, Thrombopoietin measurement in thrombocytosis: Dysregulation and lack of feedback inhibition in essential thrombocythaemia, *British Journal of Haematology*, **99** (1997), 929–932.
- [24] H. Shu, L. Wang and J. Wu, Global dynamics of Nicholson's blowflies equation revisited: Onset and termination of nonlinear oscillations, *J. Differential Equations*, **255** (2013), 2565–2586.
- [25] H. Shu, L. Wang and J. Wu, Bounded global Hopf branches for stage-structured differential equations with unimodal feedback, *Nonlinearity*, **30** (2017), 943–964.

- [26] Y. Song and J. Jiang, Steady-state, Hopf and steady-state-hopf bifurcations in delay differential equations with applications to a damped harmonic oscillator with delay feedback, *International Journal of Bifurcation and Chaos*, **22** (2012).
- [27] M.-F. Tsan, Kinetics and distribution of platelets in man, *American Journal of Hematology*, **17** (1984), 97–104.

Received December 2018; revised March 2019.

*E-mail address:* [lois.boullu@inria.fr](mailto:lois.boullu@inria.fr)

*E-mail address:* [pujo@math.univ-lyon1.fr](mailto:pujo@math.univ-lyon1.fr)

*E-mail address:* [belair@dms.umontreal.ca](mailto:belair@dms.umontreal.ca)